Hindawi
Shock and Vibration
Volume 2019, Article ID 7607214, 13 pages
https://doi.org/10.1155/2019/7607214

Research Article

Online Monitoring of Flexural Damage Index of a Cable-Stayed Bridge

Byeong Hwa Kim

Department of Civil Engineering, Kyungnam University, Changwon 51767, Republic of Korea

Correspondence should be addressed to Byeong Hwa Kim; bhkim@kyungnam.ac.kr

Received 25 July 2019; Revised 1 October 2019; Accepted 4 November 2019; Published 23 November 2019

Guest Editor: Franco Concli

This work introduces a recent application of the online nondestructive damage assessment system into a cable-stayed bridge. A set of ambient modal parameters are automatically extracted every 20 minutes using real-time signal data collected from a total of 26 accelerometers attached on the deck plate of the bridge. Then, a set of modal flexibilities are reconstructed by the combination of the extracted modal parameters with the approximated modal mass of the girder. Next, the curvature of the modal flexibility is approximated by a central difference formula. Finally, the set of flexural damage index equations is constructed by comparing the modal curvature of the damaged state to that of the undamaged state. Solving the overdetermined flexural damage index equations, the desired damage index is finally quantified. The resulting index clearly indicates the location and severity of the potential structural damage on the girder. Based on the overall performance of the implemented health monitoring system, the bridge operator's damage index control criteria are set to ±20% of the undamaged state.

1. Introduction

Long span bridges are a key component of the nation's ground transportation infrastructure network. The bridge's service life may be shortened due to various hostile environmental conditions. Bridges must be regularly inspected and maintained to provide a satisfactory level of service during the design and operation period.

Commonly used inspection techniques include visual inspection, acoustic emission, ultrasonic, radiography, eddy current, and magnetic particle inspection. These inspection methods, the so-called local methods, require the bridge inspector to access the bridge component. However, access to bridge components may be difficult in practice. Furthermore, the application of the local inspection methods to the entire bridge is not very practical. These inaccessibility and scope issues were common topics at many technical conferences and seminars related to bridge maintenance and rehabilitation.

The vibration-based nondestructive damage evaluation (NDE) approaches have received increasing attention in civil engineering due to the potential for solving the inaccessibility and scope issues of the abovementioned localized experimental inspection methods. Numerous research papers related to the vibration-based NDE methods have been published in the literature since the late 1970s.

A typical schematic of a vibration-based NDE scheme consists of the following four steps: First, the vibration response of a structure is measured. Only the output response of the structure caused by ambient excitation sources such as wind loads, normal traffic, and wave loads is measured. Second, modal analysis is performed to extract modal parameters such as mode shape, natural frequency, and damping ratio from the measured time histories. Third, using previously estimated modal parameters, various algorithms are applied to detect the location and size of damage nondestructively. Finally, a reliability or safety analysis is performed to determine the future use of the structure using the estimated results of the location and the severity of the damage.

However, the vibration-based NDE method inherently suffers from the incompleteness of the modal data generated. Here, the incompleteness of modal data may be classified into the following three categories. First, only a few of the

lower modes can be reliably estimated using existing modal analysis techniques. Second, in real bridges which all have, theoretically, an infinite number of degrees of freedom, all degrees of freedom cannot be measured. Finally, the mode shape of a structure must be sampled at the specified sensor interval. Measuring higher modes with coarse sensor intervals may not be feasible or practical.

To overcome the above shortcomings, vibration-based NDE algorithms have evolved over the past four decades. The NDE methods developed so far can be classified into the following four categories [1]. The first category provides qualitative indicators that the structure may be damaged. The second provides information on probable locations of the damage. The third provides information on the location and size of the damage, and the fourth provides information on the safety or useful life of the structure in the damaged state.

Many reviews [1–7] on vibration-based NDE methods show that the mode shape curvature (MSC) method by Pandey et al. [8] and the damage index (DI) method by Stubbs and Kim [9] accurately detect the location and severity of the damage.

The MSC method utilizes a well-known relationship between the mode shape curvature (κ) and flexural rigidity (EI) of beam cross section as given by

$$\kappa = \frac{M}{(\mathrm{EI})}, \tag{1}$$

where M denotes bending moment of the section. When structural damage is introduced, the flexural rigidity of the damaged region is reduced, increasing the magnitude of the curvature in that section of the structure. The mode shape curvatures of damaged and undamaged states are obtained through a central difference formula. The MSC method uses the absolute difference between damaged and undamaged curvatures. Because of the high sensitivity to structural damage, much research has been carried out on the MSC methods for beam-like structures [10–31]. However, there are at least three distinct disadvantages to the MSC methods [10]. First, the estimation results may vary depending on the mode; second, the singularity problems occurs near the inflection points of the mode shape; and third, a large quantity of sensors is needed to accurately estimate the curvature through the central difference formula.

To resolve the mode selection problem, it is recommended to use modal flexibility instead of the mode shape itself. Here, modal flexibility can be easily reconstructed by linear combination of mode shape and frequency. In addition, the method of using a pseudoinverse can be considered as a solution to the singularity problem. To resolve first and second drawbacks of the MSC method, the flexural damage index equation (FDIE) method [10–14] and the nodal curvature method [15, 16] are proposed. These approaches assume the so-called small damage assumption that the stresses in the deformed configuration are constant during a change of strain due to a small damage event:

$$\sigma = \sigma^*, \tag{2}$$

where the asterisk denotes a damaged state. This assumption leads to a set of flexural damage equations:

$$\boldsymbol{\Lambda\beta} = \boldsymbol{\kappa}^*, \tag{3}$$

where $\boldsymbol{\beta}$ is the damage index vector to be evaluated and $\boldsymbol{\kappa}^*$ is the curvature vector of the damaged structure. The term $\boldsymbol{\Lambda}$ denotes the curvature matrix for an undamaged structure. The FDIE is inherently an overdetermined equation. The pseudoinverse solution of equation (3) can be easily obtained by a well-known singular value decomposition procedure. The scalar element in the identified damage index vector $\boldsymbol{\beta}$ is called a damage index β. The identified damage index, β, represents the ratio of the modulus of elasticity E in the undamaged state to that in the damaged state E^*:

$$\beta \equiv \frac{E}{E^*}. \tag{4}$$

Besides the FDIE methods, various attempts have been made to resolve the singularity problem of the MSC method [17–22].

As an attempt [23–26] to resolve the third drawback of the MSC method, a method using the strain mode shape has been proposed. To extract the strain mode shape, a fiber-optic Bragg grating (FBG) sensor is used instead of the deflection mode shape extraction method using an existing accelerometer. Since the curvature is directly proportional to the strain at the flexural member, the extraction of the strain mode shape can be a good solution to the spatial resolution problem caused by the central difference process of deflection. Thanks to the availability of low-cost strain sensors, a recent study has shown theoretical and experimental success in measuring modal curvature variation directly using strain sensors and localizing various damage scenarios [27].

Recently, application studies on the damage assessment algorithms for real-time structural health monitoring (SHM) systems on the bridge have attracted special attention [28, 29]. The performance of the MSC and DI methods has been verified by several independent researchers in the laboratory as well as in field [1, 3, 4]. Although many full-scale deployments [30–33] of the vibration-based NDE methods have been reported, only the DI method shows applicability to real-time SHM systems [31, 32]. This study introduces, for the first time, the full-scale field application of the FDIE method to an online SHM system.

2. Vibration-Based NDE System

2.1. Damage Monitoring System. A vibration-based NDE system was installed on the 2nd Penang cable-stayed bridge located in Malaysia. The bridge has a total length of 475 m, a midspan of 240 m, and a clearance height of 30 m above sea level, as shown in Figure 1. The bridge deck was made of concrete. It is noted that there is no cross beam between dual-pylons of the bridge. The bridge has a dual carriageway with two lanes and a motorcycle lane on either side. The approach spans have a width of 29.8 m, and main navigation spans are 35.6 m wide.

The overall configuration of an installed NDE system is shown in Figure 2. For output-only ambient modal analysis,

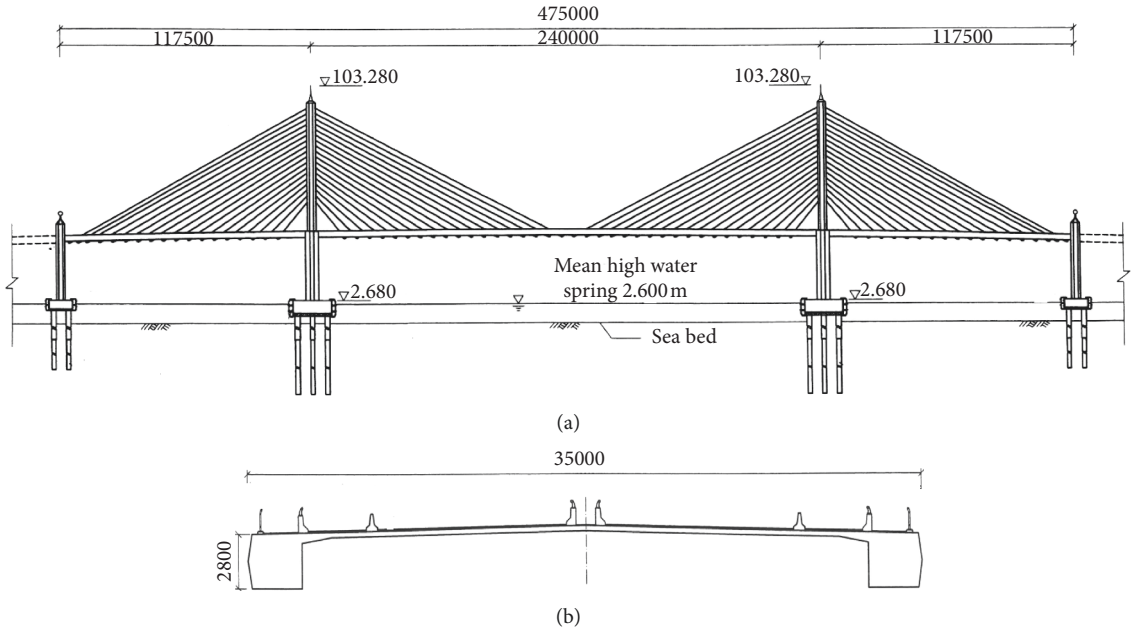

Figure 1: (a) Elevation and (b) cross section of a cable-stayed bridge.

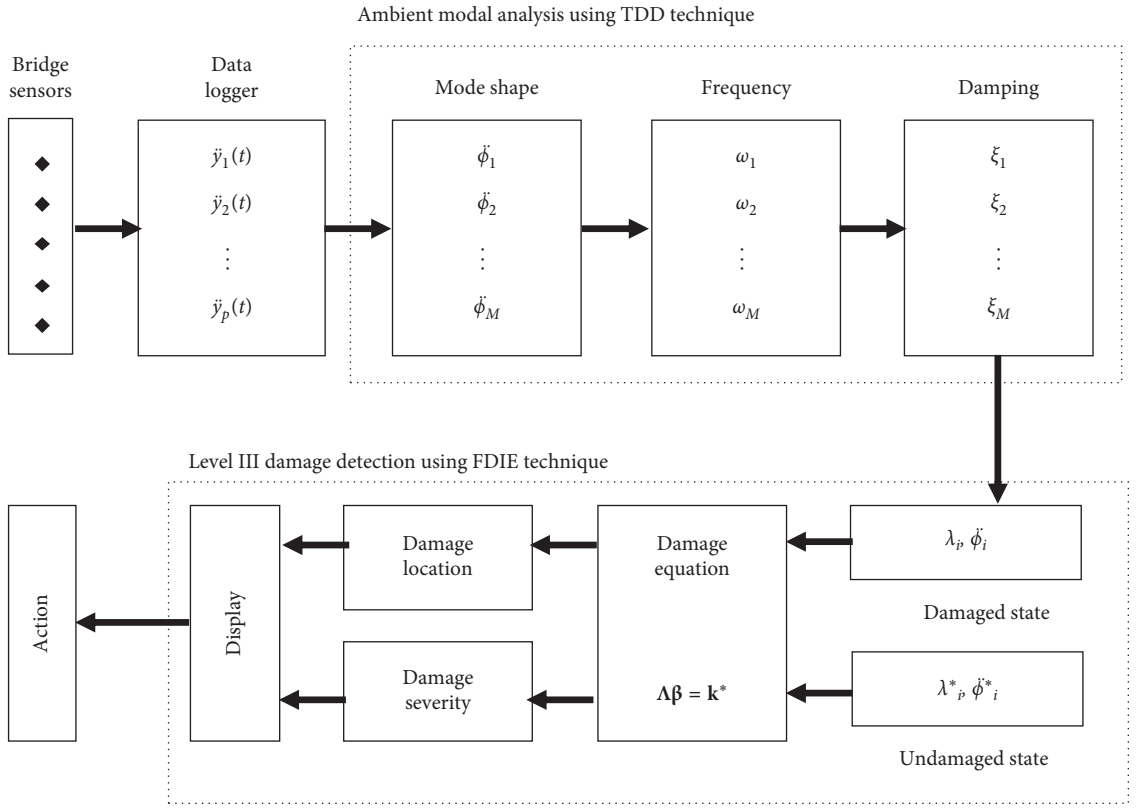

Figure 2: Overall scheme of the implemented NDE system.

time domain decomposition (TDD) technique by Kim et al. [34, 35] has been adopted because of its practicability and accuracy. The NDE method embedded in the system is the FDIE method by Kim et al. [10, 11]. The applied NDE method can be classified as the third category because it can evaluate the location and severity of the structural damage simultaneously. The first set of online ambient vibration data was collected on June 6, 2015. These data were defined as an undamaged state. The online data collected after the first data are defined as a damaged state.

The sensor layouts are shown in Figure 3. Here, the terms "EB" and "WB" in the sensor numbers indicate the east and west bound direction, respectively. The Z and Y coordinates indicate the vertical and lateral direction, respectively, while the X coordinate represents the axial direction of the bridge. As shown in Figure 3, a total of 26 three-axial accelerometers are used. The output only time responses at the 26 nodes due to normal traffic volume and wind load have been measured for two hours with a sampling frequency of 100 Hz.

The accelerometers and data acquisition system were installed on the deck plate of the bridge, and the data server was installed in the office as shown in Figure 4. The accelerometer was installed at the top of a newly constructed mortar block to avoid damage due to intensive rainfall. The data acquisition system was installed near the concrete pylon and protected by a steel cabinet to prevent possible vandalism. The network protocol (NTP) server collects and stores various signals, such as cable tension, strains, thermometers, and GPS, into the SHM system as well as the NDE system in real time.

The vibration-based NDE system software performs ambient modal analysis by applying the TDD technique to real-time data received from the NTP server every 20 minutes. Then, the damage index is extracted by applying the FDIE method to the modal parameters as shown in Figure 5. Finally, the extracted damage index is stored in the SHM database.

3. Ambient Modal Analysis

3.1. Inspection of Measured Signals. Typical acceleration time histories at the east bound in the Z and Y directions at the center of the main span are shown in Figure 6. It is seen that normal traffic volume excites the bridge deck plate transversely in the range of 4 gal (cm/s^2). However, the amplitude of lateral vibration of the deck is at most 2 gal. This implies that the mode in the Y direction can be hardly excited by the normal traffic load.

It is well known that modal analysis is based on linear theory. The aspect ratio is very large, allowing the deck to be modelled as a slender beam. The vertical components are orthogonal to the horizontal components and independent of each other. The structural responses are also different because the governing equations, cross-sectional stiffness, boundary conditions, and excitations are different for the horizontal and vertical directions. Thus, it is clear that horizontal structural damage is identified from the horizontal response and vertical structural damage is identified from the vertical response. Here, the vertical structural damage and the horizontal structural damage literally mean structural damage identified in the vertical and horizontal direction, respectively. The main source of excitation for the deck is normal traffic, not ambient wind loads. A time spike occurs when the vehicle passes the sensor. It is noted that time response is the sum of many steady-state natural modes and excitation modes. After the time domain observation of the amplitude of spikes, the magnitude of modes in frequency domain cannot be quantified. The position of the time spikes coincides in the vertical and horizontal directions, as shown in Figure 6. It can be expected that the vertical excitation to be much stronger than the horizontal excitation under normal conditions. On the other hand, the horizontal stiffness of the deck plate is much greater than the vertical stiffness, as shown in Figure 1(a). It is noted that only three horizontal modes are excited in the horizontal direction while nine modes are excited in the vertical direction within 1.5 Hz. Therefore, it makes sense to assume that we are more likely to find structural damage using vertical components than horizontal ones. This is because the reliability of modal parameters extracted from the horizontal direction is much lower than that of the vertical direction due to the weaker excitation to higher stiffness direction. Rather, taking into account horizontal components can lower the confidence of the estimated damage result. For this reason, only vertical components are considered, horizontal components are not intentionally considered in the procedure of damage estimation.

Based on this fact, the acceleration data collected only in the Z direction were used in the following NDE schemes.

The acceleration responses collected in the Z and Y direction at the west bound WB7 node are shown in Figure 7. It is observed that the average acceleration collected from the west bound sensor tends to drift up at zero, while the east bound acceleration remains at zero. It is suspected that the sensors installed on the west bound may have some problems with this performance. The detrending process subtracts the mean- or best-fit line from the data in the least-square sense. The detrending process is only suitable for frequency extraction and has a problem with mode shape extraction. Different average values for different sensors can reduce the accuracy of mode shape estimation. For this reason, the detrending technique was not used for this task.

All the power spectra of all the acceleration time responses in the Z direction are superimposed in Figure 8(a). To draw the spectrum, the Hanning window is used and the NFFT parameter is set to 2^{10}. Frequency resolution is 0.0061 Hz. The average spectrum of the frequency band 0 to 1.5 Hz is shown in Figure 8(b). It is seen that a total of 9 transverse modes are excited up to 1.5 Hz and the modes are well separated.

3.2. Extraction of Modal Parameters Using TDD Technique. The TDD technique [34, 35] extracts the spatial variables (mode shapes) and the temporal parameters (frequency and damping) separately. A flow chart of the TDD technique is shown in Figure 9. First of all, a set of the digital band pass filters must be designed to extract a set of single-degree-of-freedom (SDOF) signals from a measured multidegree-of-freedom (MDOF) signal. Here, the ranges of the pass bands are easily identified by visually inspecting Figure 8 in detail. Digital band pass filtering allows for a set of the SDOF signals. Next, for each mode, a set of mode isolated signal matrices $\mathbf{Y}_i$ must be constructed. A simple multiplication of the mode separated signal matrix then yields the energy matrix $\mathbf{E}_i$ for each mode. Finally, the ith mode shape is taken

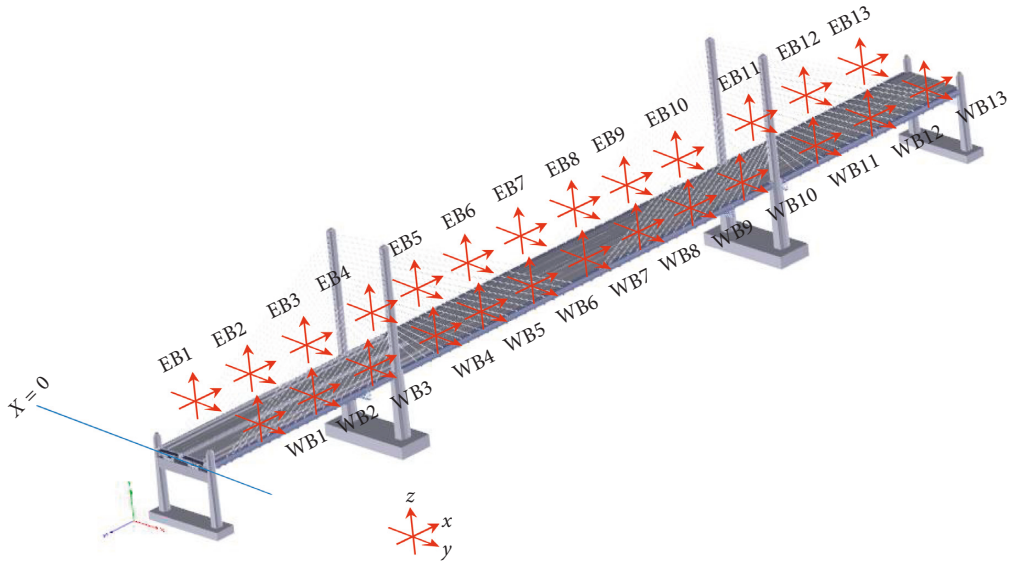

Figure 3: Sensor deployment of the online SHM system (3D view).

(a) (b) (c)

Figure 4: Online SHM system. (a) Accelerometer. (b) Data acquisition system. (c) NTP server.

by singular value decomposition (SVD) for the energy matrix $\mathbf{E}_i$ and then by the first column of the singular vector matrix $\mathbf{U}_i$.

The extracted first mode shape in the transverse Z direction is shown Figure 10. All the identified modal parameters are listed in Table 1.

For the eigenvalue analysis, a 3D finite element (FE) model has been constructed by a commercial software MIDAS [36], as shown in Figure 11. Total 671 nodes and 614 elements are used in the numerical model. The deck plate, pylon, and piles are modelled by 470 composite beam elements, while the inclined cables are modelled by 144 cable elements with certain tension.

The identified mode shapes of the FE model are shown in Figure 12. Comparing the identified mode shapes, the numerical FE model has only a few modes, as shown in Table 1. There are several missing modes on the FE model, and only 6 modes are available for the vertical mode in the 1.5 Hz range. The missing modes are due to the simplicity of the numerical model. If plate elements are used for the deck plate instead of beam elements, one may find more complex modes in lower modes. However, this significantly increases the amount of work that needs to be analyzed.

The first bending mode of the FE model occurs at 0.4207 Hz and is very close to the first bending mode 0.3988 Hz measured. In addition, the first mode shape of the

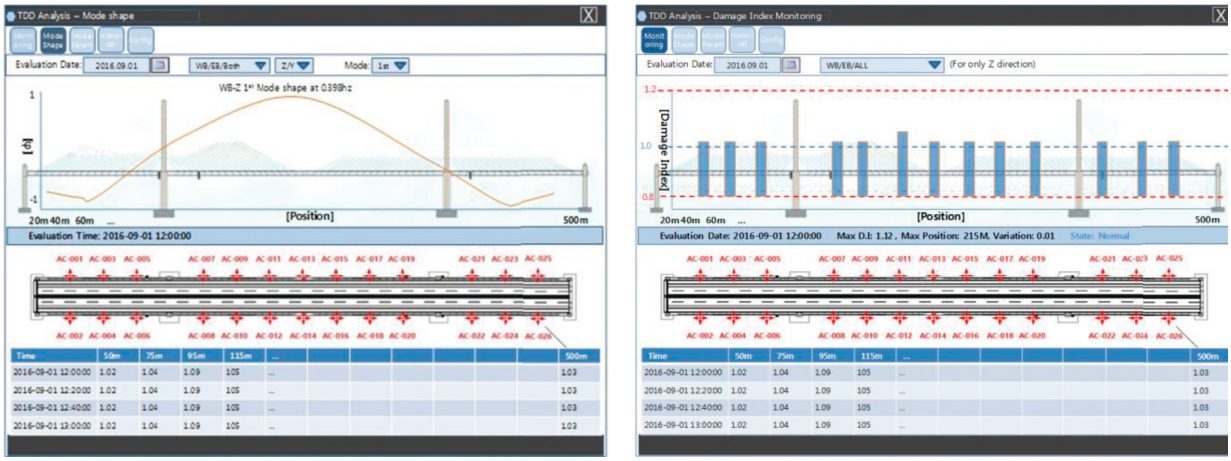

(a) (b)

Figure 5: Vibration-based NDE system software. (a) Ambient modal analysis. (b) FDIE analysis.

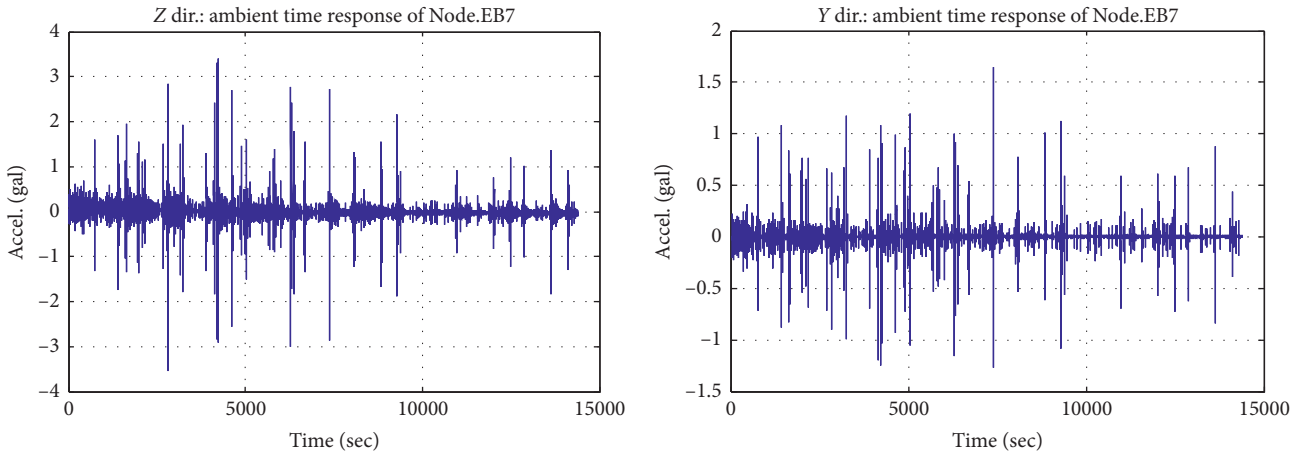

(a) (b)

Figure 6: Acceleration time histories at Node EB7. (a) Z direction. (b) Y direction.

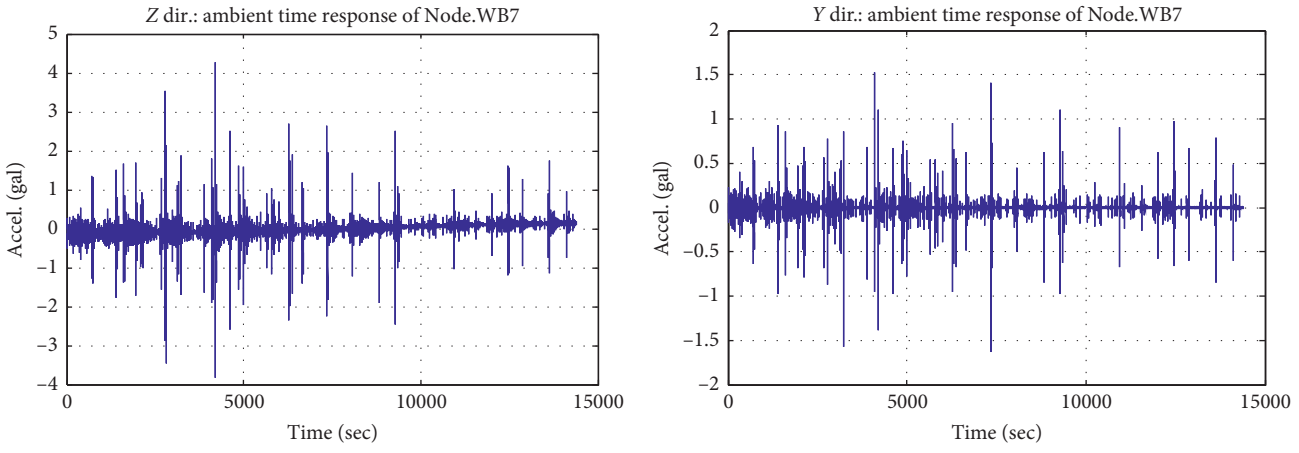

(a) (b)

Figure 7: Acceleration time histories at Node WB7. (a) Z direction. (b) Y direction.

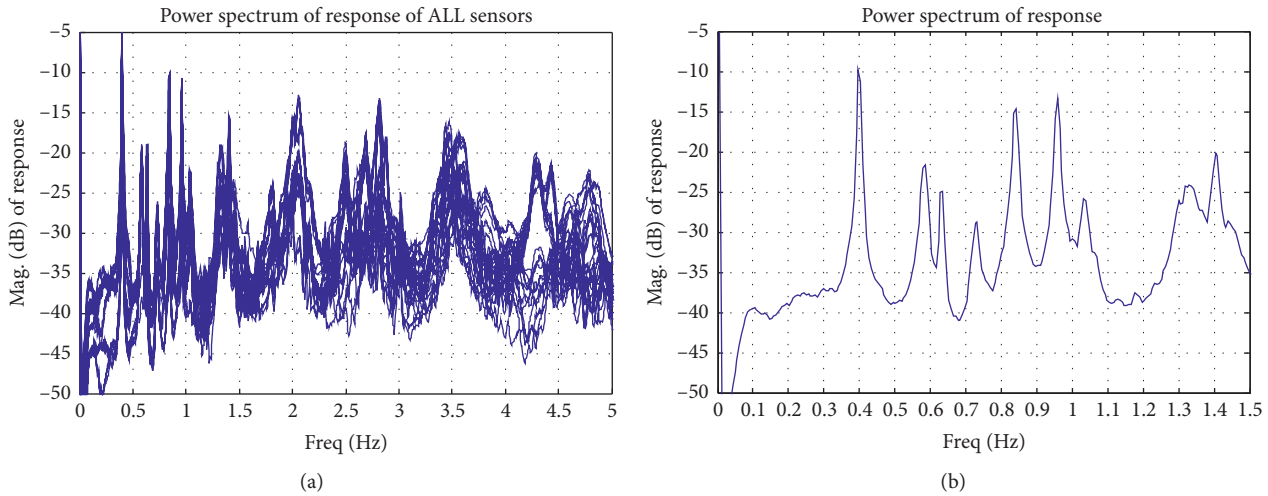

Figure 8: Power spectrum of all the acceleration time histories. (a) Overlapped. (b) Averaged.

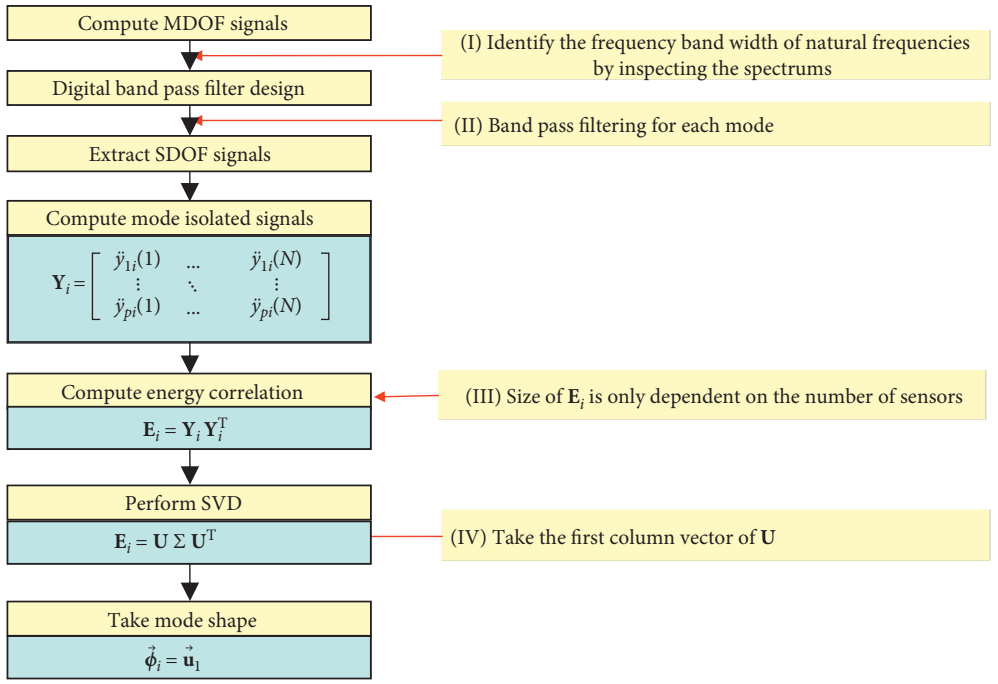

Figure 9: TDD technique.

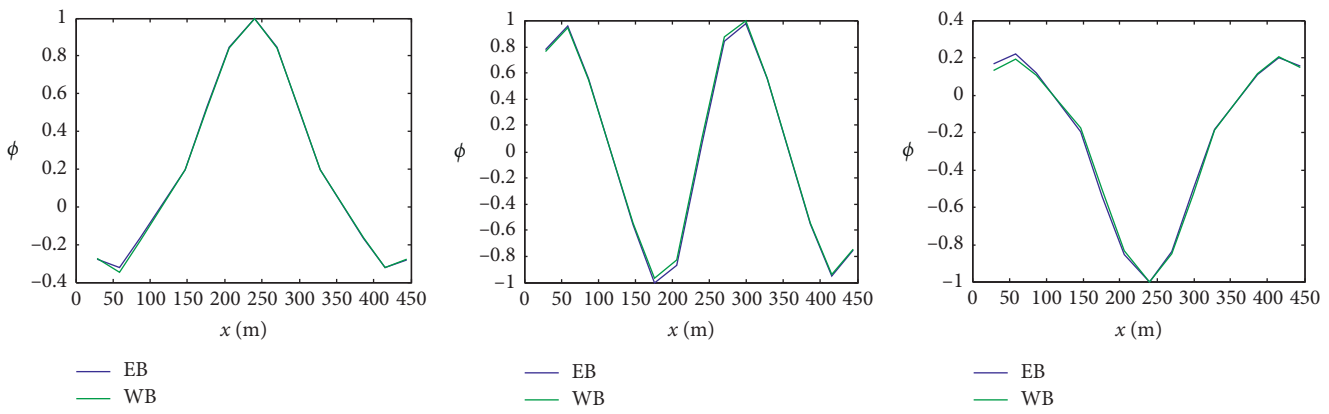

Figure 10: Continued.

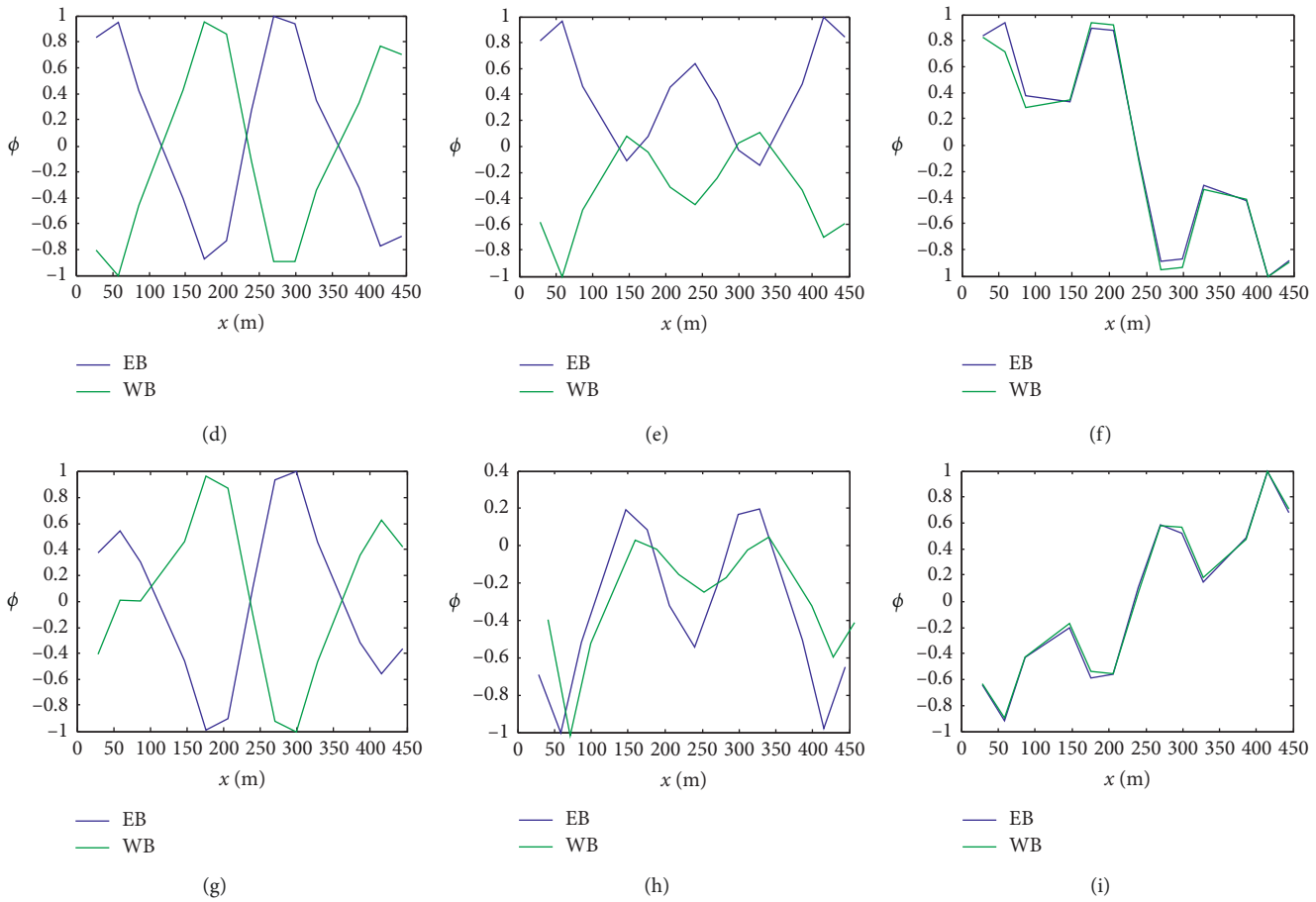

Figure 10: Identified nine lower mode shapes. (a) First. (b) Second. (c) Third. (d) Fourth. (e) Fifth. (f) Sixth. (g) Seventh. (h) Eighth. (i) Ninth.

Table 1: Identified temporal parameters in Z direction.

Mode no.	FE model freq. (Hz)	Measured				
		Peak-picking freq. (Hz)	TDD		Modal mass $\times 10^4$ (kg/m)	
			Undamped freq. (Hz)	Damping ratio (%)	EB	WB
1	0.4207	0.3967	0.3988	0.1069	0.8577	0.8595
2	0.4943	0.5798	0.5829	0.2906	1.7323	1.6944
3	—	0.6287	0.6319	0.1259	0.8069	0.7949
4	0.7236	0.7263	0.7291	0.3199	1.4580	1.4915
5	0.9122	0.8362	0.8389	0.1801	0.9864	0.6638
6	1.0522	0.9521	0.9576	0.1072	1.5557	1.5371
7	—	1.0310	1.0396	0.3118	1.2175	1.1147
8	1.3238	1.3310	1.3141	0.3468	0.8986	0.5070
9	—	1.4100	1.4055	0.1801	1.0299	1.0110

FE model shown in Figure 12(a) is very similar to the measurement mode shown in Figure 10(a). In mode shape, the second bend mode 0.4943 Hz of the FE model is very similar to the second measurement mode 0.5798 Hz. The fourth and fifth measurement modes are twisting modes and appear in the third and fourth modes in the FE model. The fifth and sixth mode shapes of the FE model shown in Figure 12 are similar to the measured sixth and eighth mode shapes shown in Figure 10. In Figure 12, the bending mode shape in the east bound direction is the same as that of the mode shape in the west bound.

4. Damage Index from FDIE Method

To evaluate structural damage, a set of the jth modal flexibility should be extracted for both damaged and undamaged

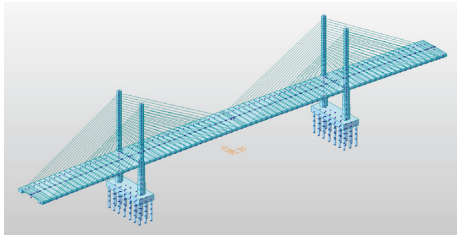

Figure 11: Overview of the FE model.

states. Here, the undamaged state is defined as a structural condition on June 6, 2016, and thereafter it is defined as a damaged state. Thus, the modal parameters and modal flexibilities presented in the previous section are considered as an undamaged state. Meanwhile, the 20-minute data collected by the online health monitoring system are considered as a damaged state. For the 20-minute online data, the ambient modal analysis should be repeated automatically.

The structural damage evaluation procedure is performed only in the transverse Z direction. This is because the damage assessment using the lateral Y signal is less reliable than the damage assessment using the transverse Z signal.

The FDIE [10–14] method has been applied to nondestructively evaluate the structural damage on the girder. The overall scheme for the FDIE method is shown in Figure 13.

4.1. Extraction of Modal Flexibility. Using the measured modal parameters, the jth modal flexibility f_j can be reconstructed by the following equation:

$$f_j = \sum_{i=1}^{N} \frac{\phi_{ji}}{m_i \omega_i^2} \phi_i, \tag{5}$$

where the terms m_i, ω_i, and ϕ_i, respectively, denote the modal mass, circular natural frequency, and mode shape vector for the ith mode and the term ϕ_{ji} denotes the jth component of the vector ϕ_i. The physical meaning of the jth modal flexibility is a deflection curve when the unit load locates at the jth node.

Modal mass cannot be measured in the ambient modal analysis. However, the modal mass may be approximated numerically by the following equation [11]:

$$m_i = \int_0^L \rho A \phi_i^2 \, \mathrm{d}x, \tag{6}$$

where the terms ρ and A, respectively, denote the mass density and sectional area of the girder. After interpolating the mode shape with the cubic spline function, the numerical integration is performed with trapezoidal rules. The modal masses estimated using equation (6) are listed in the right column of Table 1. The contribution of individual modes to modal flexibility is shown in Figure 14. It is seen that the modal contributions after the fifth mode appear to be negligible.

The extracted 6th flexibility for undamaged and damaged states is compared in Figure 15. The 6th modal flexibility, f_6, represents the displacement profile when the unit load is applied to the 6th sensor position $x = 205.50$ m. There is no significant difference in modal flexibility before and after damage.

4.2. Extracting Curvature of Modal Flexibility. The curvatures of the 6th modal flexibility can be extracted through a central difference formula. The resulting curvatures are shown in Figure 16. It should be noted that the absolute error level of the modal curvature estimation is proportional to the distance between the sensors. However, the FDIE algorithm focuses on the relative difference in the modal curvature, not the absolute difference between damaged and undamaged states. As long as the distance between the sensors does not change, the error level of the modal curvature estimation does not affect the final accuracy of the results of the FDIE method.

4.3. Flexural Damage Index Equation. Using a set of the extracted curvatures for both damaged and undamaged states, the set of FDIEs is constructed as shown in equation (3). FDIE is inherently an overdetermined equation, and a pseudoinverse solution is given below.

Premultiplication of $\mathbf{\Lambda}^{\mathrm{T}}$ on both sides of equation (3) yields a reduced set of equations:

$$\mathbf{\Lambda}^{\mathrm{T}} \mathbf{\Lambda} \boldsymbol{\beta} = \mathbf{\Lambda}^{\mathrm{T}} \boldsymbol{\kappa}^{*}. \tag{7}$$

Symmetric matrix $\mathbf{\Lambda}^{\mathrm{T}}\mathbf{\Lambda}$ can be decomposed into singular value matrix $\mathbf{\Omega}$ and singular vector matrix $\mathbf{Y}$ as follows:

$$\mathbf{\Lambda}^{\mathrm{T}} \mathbf{\Lambda} = \mathbf{Y} \mathbf{\Omega} \mathbf{Y}^{\mathrm{T}}. \tag{8}$$

Then, the a *pseudoinverse* of the matrix $\mathbf{\Lambda}^{\mathrm{T}}\mathbf{\Lambda}$ satisfying all the Moore–Penrose conditions [37] is

$$\mathbf{\Gamma} = \mathbf{Y} \mathbf{\Omega}^{-1} \mathbf{Y}^{\mathrm{T}}. \tag{9}$$

Finally, the pseudoinverse solution for overdetermined FDIEs is known by the following equation:

$$\boldsymbol{\beta} = \mathbf{Y} \mathbf{\Omega}^{-1} \mathbf{Y}^{\mathrm{T}} \mathbf{\Lambda} \boldsymbol{\kappa}^{*}. \tag{10}$$

For the data set collected at the east bound, the damage index identified by FDIEs is shown in Figure 17(a). A positive peak above the number "1" indicates the location and severity of the suspected damage. This result shows that the calculated damage index is near 1. This means that there is no structural damage to the location.

For the west bound data, the NDE procedure mentioned above was repeated. The identified damage index is shown in Figure 17(b). It can be seen that the damage index shows a large variation near the boundary. This relatively large error on the estimated damage index is due to the performance issues of the sensor mentioned previously. Recall that the average of the acceleration measured at the west bound is not zero, as shown in Figure 7. These abnormalities in the sensor performance were investigated and corrected later.

The final representative damage index for the deck plate can be obtained by averaging the two indices as shown in Figure 18. The dotted lines indicate the recommended

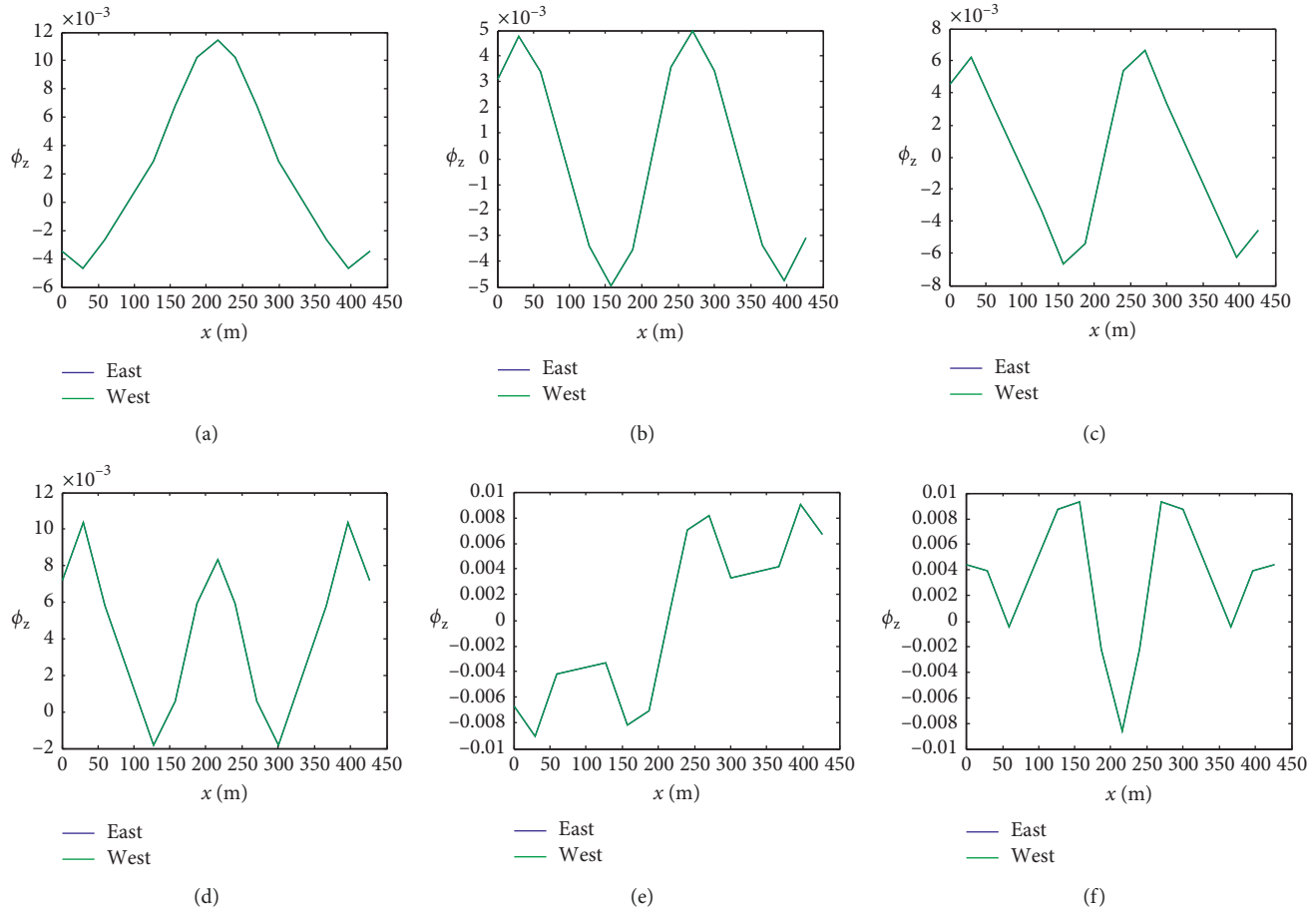

Figure 12: First six lower bending mode shapes of the FE model. (a) First. (b) Second. (c) Third. (d) Fourth. (e) Fifth. (f) Sixth.

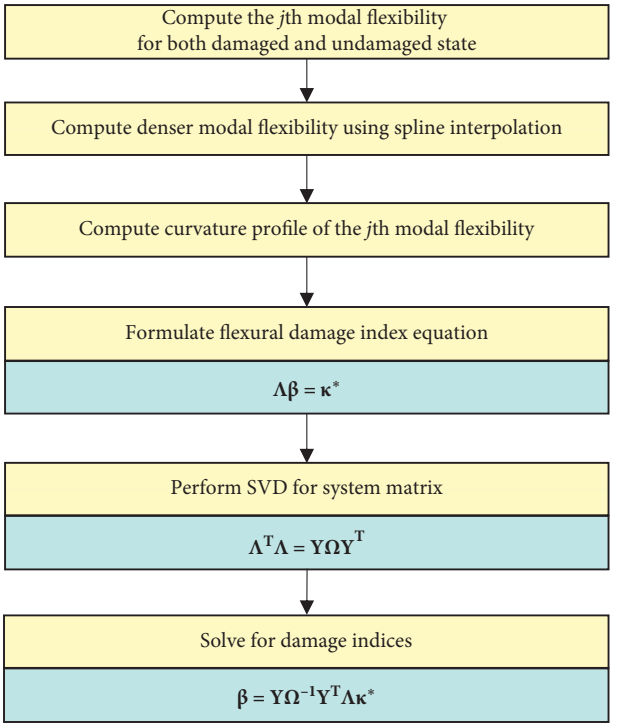

Figure 13: FDIE method.

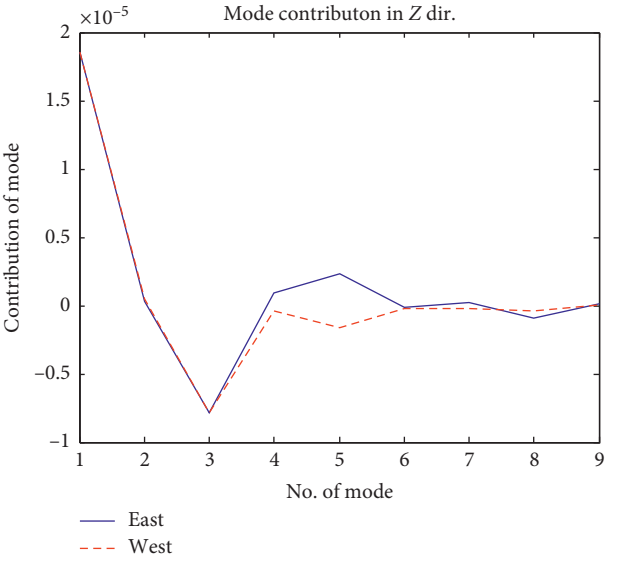

Figure 14: Contribution of modes to modal flexibility in the Z direction.

accuracy range. Assuming there is no possibility of damage to the deck plate during this measurement activity, the current NDE system implemented can evaluate structural

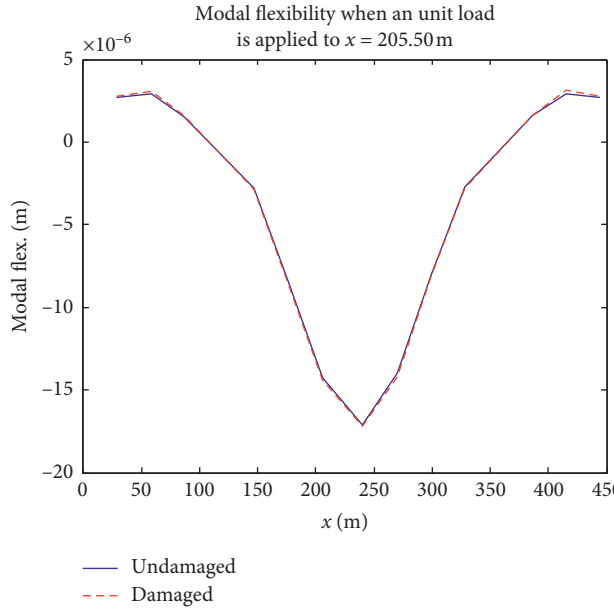

Figure 15: The 6th modal flexibility extracted in the Z direction ($j = 6$).

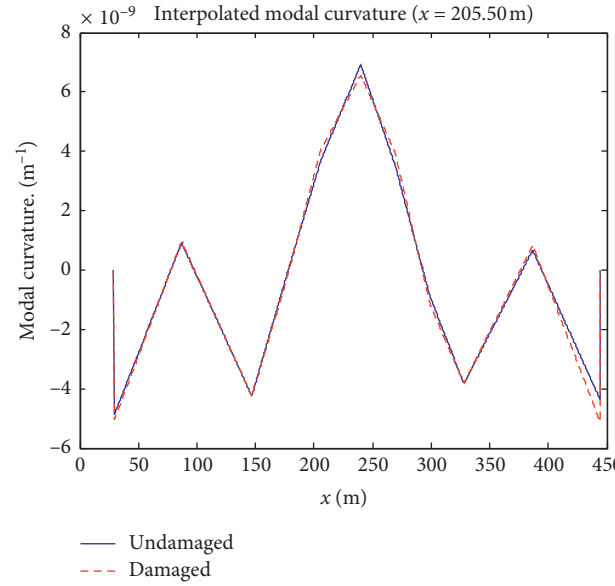

Figure 16: Curvature of the extracted modal flexibility ($J = 6$).

damage in the accuracy range of about 20%. Typically, the signal measurement error is about 5% and the numerical modelling error is about 10%. It is also pointed out that the safety factor for structural design for various uncertainties is about 20%. Based on concerns about the various levels of errors and overall uncertainty on the hostile environment of the NDE system, the level of control of the damage index of the implemented NDE system was set at 20%. If the damage index is below 0.8, the NDE software or sensor must be checked out. If the damage index is 1.2 or more, the structural safety maintenance inspector must be dispatched to the designated location for a detailed safety inspection.

5. Summary and Conclusions

An online vibration-based NDE system has been successfully implemented on the deck plate of a cable-stayed bridge. The implemented NDE method is the FDIE method. The structural damage of the deck plate was monitored every 20 minutes using real-time online data. The TDD technique has been implemented to extract modal parameters from output-only online signals. After the modal flexibility is reconstructed from the extracted modal parameters, a curvature set is obtained through a central difference formula. Next, a set of flexural damage index equations is constructed and the damage index is estimated.

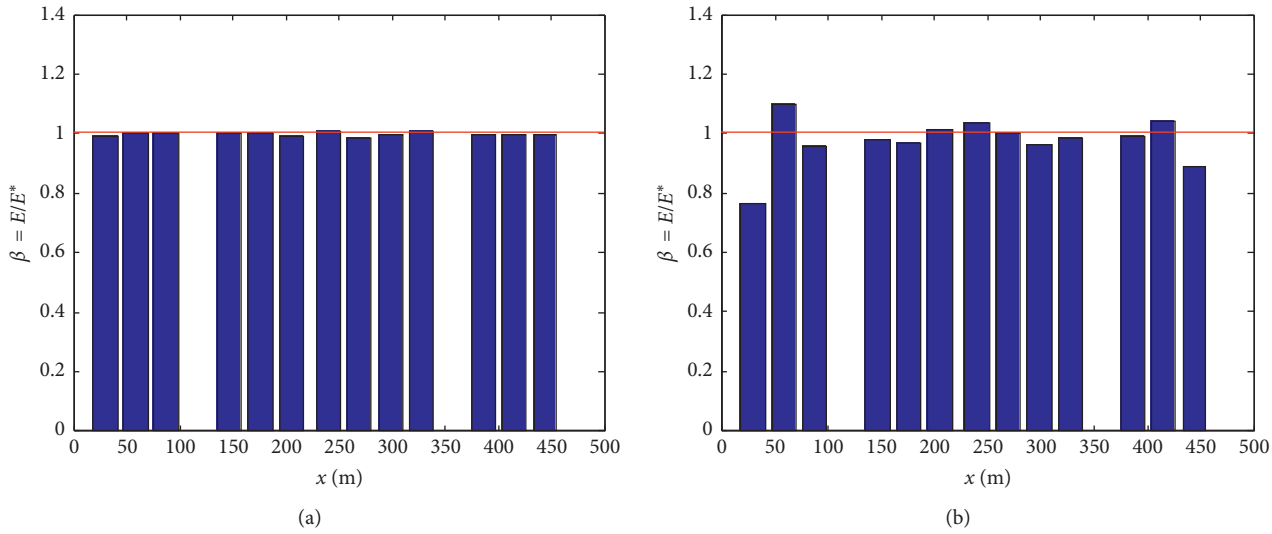

Figure 17: Identified damage index of the deck plate. (a) East bound. (b) West bound.

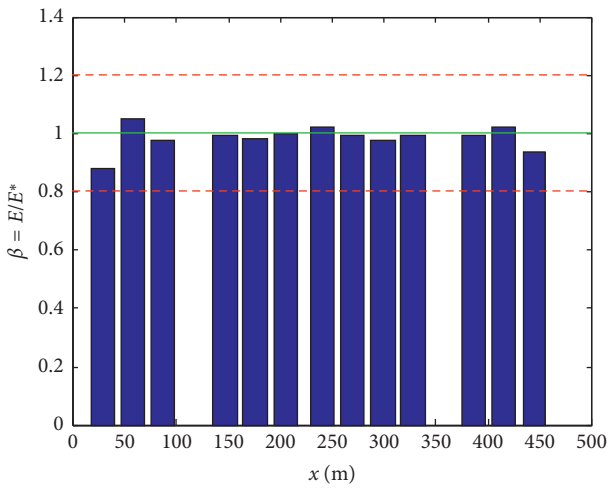

Figure 18: Representative damage index of the deck plate (average).

Based on the performance of the implemented NDE system, the following four conclusions could be drawn:

First, the fault in a sensor can be misinterpreted as structural damage. After the sensor is first installed, it must be periodically calibrated to ensure that the system remains stable.

Second, it is necessary to extract accurate modal parameters from the big data measured in real time from a large number of sensors in a short time. Also, it is very advantageous to separate temporal and spatial variables like the TDD method.

Third, for the maintenance of bridges, a range of management of damage index is needed. To determine the extent of management of the damage index, the various error levels of the entire system process should be considered.

Finally, the FDIE method is applicable to the online real-time NDE system. This study demonstrates for the first time the field application of the FDIE method to the online SHM system.

Data Availability

The time history data used to support the findings of this study are available from the corresponding author upon request.

Conflicts of Interest

The author declares that there are no conflicts of interest regarding the publication of this paper.

Acknowledgments

This research was supported by the fund of Kyungnam University.

References

[1] S. W. Doebling, C. R. Farrar, and M. B. Prime, "A summary review of vibration-based damage identification methods," *The Shock and Vibration Digest*, vol. 30, no. 2, pp. 91–105, 1998.

[2] E. P. Carden and P. Fanning, "Vibration based condition monitoring: a review," *Structural Health Monitoring: An International Journal*, vol. 3, no. 4, pp. 355–377, 2004.

[3] W. Fan and P. Qiao, "Vibration-based identification methods: a review and comparative study," *Structural Health Monitoring: An International Journal*, vol. 10, no. 1, pp. 83–111, 2011.

[4] D. Dessi and G. Camerlengo, "Damage identification techniques via modal curvature analysis: overview and comparison," *Mechanical Systems and Signal Processing*, vol. 52-53, pp. 181–205, 2015.

[5] S. Das, P. Saha, and S. K. Patro, "Vibration-based damage detection techniques used for health monitoring of structures: a review," *Journal of Civil Structural Health Monitoring*, vol. 6, no. 3, pp. 477–507, 2016.

[6] J. R. Casas and J. J. Moughty, "Bridge damage detection based on vibration data: past and new developments," *Frontiers in Built Environment*, vol. 3, no. 4, pp. 1–12, 2017.

[7] G. F. Gomes, Y. A. D. Mendez, P. S. L. Alexandrino, S. S. Cunha, and A. C. Ancelotti, "A Review of vibration based inverse methods for damage detection and identification in mechanical structures using optimization algorithms and ANN," *Archives of Computational Methods in Engineering*, vol. 26, no. 4, pp. 883–897, 2019.

[8] A. K. Pandey, M. Biswas, and M. M. Samman, "Damage detection from changes in curvature mode shapes," *Journal of Sound and Vibration*, vol. 145, no. 2, pp. 321–332, 1991.

[9] N. Stubbs and J.-T. Kim, "Damage localization in structures without baseline modal parameters," *AIAA Journal*, vol. 34, no. 8, pp. 1644–1649, 1996.

[10] D. Y. Kim, J. K. Joo, Y. K. Park, S. Y. Ryu, Y. J. Kim, and S. K. Kim, "Prognostic factors in gastric carcinoma with peritoneal dissemination," *Acta Chirurgica Belgica*, vol. 106, no. 6, pp. 665–668, 2006.

[11] B. H. Kim, N. Stubbs, and T. Park, "Flexural damage index equations of a plate," *Journal of Sound and Vibration*, vol. 283, no. 1-2, pp. 341–368, 2005.

[12] B. H. Kim, H. J. Joo, and T. Park, "Damage evaluation of an axially loaded beam using modal flexibility," *KSCE Journal of Civil Engineering*, vol. 11, no. 2, pp. 101–110, 2007.

[13] B. H. Kim, T. Park, and G. Z. Voyiadjis, "Damage estimation on beam-like structures using the multi-resolution analysis," *International Journal of Solids and Structures*, vol. 43, no. 14-15, pp. 4238–4257, 2006.

[14] B. H. Kim, H. Kim, and T. Park, "Nondestructive damage evaluation of plates using the multi-resolution analysis of two-dimensional haar wavelet," *Journal of Sound and Vibration*, vol. 292, no. 1-2, pp. 82–104, 2006.

[15] S. Dincal and N. Stubbs, "Nondestructive damage detection in Euler-Bernoulli beams using nodal curvatures-part I: theory and numerical verification," *Structural Control and Health Monitoring*, vol. 21, no. 3, pp. 303–316, 2014.

[16] S. Dincal and N. Stubbs, "Nondestructive damage detection in Euler-Bernoulli beams using nodal curvatures-part II: field measurements," *Structural Control and Health Monitoring*, vol. 21, no. 3, pp. 331–341, 2014.

[17] M. Cao, M. Radzieński, W. Xu, and W. Ostachowicz, "Identification of multiple damage in beams based on robust curvature mode shapes," *Mechanical Systems and Signal Processing*, vol. 46, no. 2, pp. 468–480, 2014.

[18] Y. F. Xu, W. D. Zhu, J. Liu, and Y. M. Shao, "Identification of embedded horizontal cracks in beams using measured mode shapes," *Journal of Sound and Vibration*, vol. 333, no. 23, pp. 6273–6294, 2014.

[19] R. Janeliukstis, S. Rucevskis, M. Wesolowski, and A. Chate, "Experimental structural damage localization in beam structure using spatial continuous wavelet transform and mode shape curvature methods," *Measurement*, vol. 102, pp. 253–270, 2017.

[20] M. Cao and P. Qiao, "Novel Laplacian scheme and multi-resolution modal curvatures for structural damage identification," *Mechanical Systems and Signal Processing*, vol. 23, no. 4, pp. 1223–1242, 2009.

[21] Z.-B. Yang, M. Radzienski, P. Kudela, and W. Ostachowicz, "Fourier spectral-based modal curvature analysis and its application to damage detection in beams," *Mechanical Systems and Signal Processing*, vol. 84, pp. 763–781, 2017.

[22] J. Ciambella, A. Pau, and F. Vestroni, "Effective filtering of modal curvatures for damage identification in beams," *Procedia Engineering*, vol. 199, pp. 1876–1881, 2017.

[23] M. Chandrashekhar and R. Ganguli, "Damage assessment of structures with uncertainty by using mode-shape curvatures and fuzzy logic," *Journal of Sound and Vibration*, vol. 326, no. 3–5, pp. 939–957, 2009.

[24] D. Anastasopoulos, P. Moretti, T. Geernaert et al., "Identification of modal strains using sub-microstrain FBG data and a novel wavelength-shift detection algorithm," *Mechanical Systems and Signal Processing*, vol. 86, pp. 58–74, 2017.

[25] D. Anastasopoulos, M. De Smedt, L. Vandewalle, G. De Roeck, and E. P. B. Reynders, "Damage identification using modal strains identified from operational fiber-optic Bragg grating data," *Structural Health Monitoring*, vol. 17, no. 6, pp. 1441–1459, 2017.

[26] H. Cui, X. Xu, W. Peng, Z. Zhou, and M. Hong, "A damage detection method based on strain modes for structures under ambient excitation," *Measurement*, vol. 125, pp. 438–446, 2018.

[27] J. Ciambella, A. Pau, and F. Vestroni, "Modal curvature-based damage localization in weakly damaged continuous beams," *Mechanical Systems and Signal Processing*, vol. 121, pp. 171–182, 2019.

[28] J. Seo, J. W. Hu, and J. Lee, "Summary review of structural health monitoring applications for highway bridges," *Journal of Performance of Constructed Facilities*, vol. 30, no. 4, Article ID 04015072, 2016.

[29] M. R. Kaloop and J. W. Hu, "Stayed-cable bridge damage detection and localization based on accelerometer health monitoring measurements," *Shock and Vibration*, vol. 2015, Article ID 102680, 11 pages, 2015.

[30] H. Guan, V. M. Karbhari, and C. S. Sikorsky, "Web-based structural health monitoring of an FRP composite bridge," *Computer-Aided Civil and Infrastructure Engineering*, vol. 21, no. 1, pp. 39–56, 2006.

[31] H. Guan, V. M. Karbhari, and C. S. Sikorsky, "Long-term structural health monitoring system for a FRP composite highway bridge structure," *Journal of Intelligent Material Systems and Structures*, vol. 18, no. 8, pp. 809–823, 2007.

[32] L. S. Lee, V. M. Karbhari, and C. Sikorsky, "Structural health monitoring of CFRP strengthened bridge decks using ambient vibrations," *Structural Health Monitoring: An International Journal*, vol. 6, no. 3, pp. 199–214, 2007.

[33] J. Niu, Z. Zong, and F. Chu, "Damage identification method of girder bridges based on finite element model updating and modal strain energy," *Science China Technological Sciences*, vol. 58, no. 4, pp. 701–711, 2015.

[34] B. H. Kim, N. Stubbs, and T. Park, "A new method to extract modal parameters using output-only responses," *Journal of Sound and Vibration*, vol. 282, no. 1-2, pp. 215–230, 2005.

[35] B. H. Kim, J. Lee, and D. H. Lee, "Extracting modal parameters of high-speed railway bridge using the TDD technique," *Mechanical Systems and Signal Processing*, vol. 24, no. 3, pp. 707–720, 2010.

[36] Midas-IT, *MIDAS Civil Manual*, Navi Mumbai, India, 2016.

[37] G. H. Golub and C. F. Van Loan, *Matrix Computations*, The Johns Hopkins University Press, Baltimore, MD, USA, 3rd edition, 1996.